Journal Pre-proof

Intracardiac administration of ephrinA1-Fc preserves mitochondrial bioenergetics during acute ischemia/reperfusion injury

Maria J. Torres, Kelsey L. McLaughlin, Randall H. Renegar, Smrithi Valsaraj, K'Shylah S. Whitehurst, Omar M. Sharaf, Uma M. Sharma, Julie L. Horton, Brinda Sarathy, Justin C. Parks, Jeffrey J. Brault, Kelsey H. Fisher-Wellman, P. Darrell Neufer, Jitka A.I. Virag

PII: S0024-3205(19)30980-4

DOI: https://doi.org/10.1016/j.lfs.2019.117053

Reference: LFS 117053

To appear in: *Life Sciences*

Received Date: 12 September 2019

Revised Date: 6 November 2019

Accepted Date: 8 November 2019

Please cite this article as: M.J. Torres, K.L. McLaughlin, R.H. Renegar, S. Valsaraj, K'S.S. Whitehurst, O.M. Sharaf, U.M. Sharma, J.L. Horton, B. Sarathy, J.C. Parks, J.J. Brault, K.H. Fisher-Wellman, P.D. Neufer, J.A.I. Virag, Intracardiac administration of ephrinA1-Fc preserves mitochondrial bioenergetics during acute ischemia/reperfusion injury, *Life Sciences*, https://doi.org/10.1016/j.lfs.2019.117053.

Intracardiac administration of ephrinA1-Fc preserves mitochondrial bioenergetics during acute ischemia/reperfusion injury

Maria J. Torres[1], Kelsey L. McLaughlin[1,2], Randall H. Renegar[3], Smrithi Valsaraj[2], K'Shylah S. Whitehurst[2], Omar M. Sharaf[2], Uma M. Sharma[2], Julie L. Horton[1,2], Brinda Sarathy[2], Justin C. Parks[2], Jeffrey J. Brault[2,4], Kelsey H. Fisher-Wellman[1,2], P. Darrell Neufer[1,2], and Jitka A. I. Virag[2†].

[1]East Carolina Diabetes and Obesity Institute, East Carolina University, Greenville, NC 27834, USA.

[2]Dept of Physiology, Brody School of Medicine, East Carolina University, Greenville, NC 27834, USA.

[3]Dept of Anatomy and Cell Biology, Brody School of Medicine, East Carolina University, Greenville, NC 27834, USA.

[4]Dept of Kinesiology, College of Health and Human Performance, East Carolina University, Greenville, NC 27834, USA.

Short title: EphrinA1-Fc preserves mitochondrial function in acute I/R

† To whom correspondence should be addressed:

Jitka Virag, PhD

Department of Physiology, Brody School of Medicine, East Carolina University

600 Moye Blvd Greenville, North Carolina, USA.

Ph: 252-744-2777

e-mail: viragj@ecu.edu

ORCID ID https://orcid.org/0000-0003-3321-9861

Abstract

Aims: Intracardiac injection of recombinant EphrinA1-Fc immediately following coronary artery ligation in mice reduces infarct size in both reperfused and non-reperfused myocardium, but the cellular alterations behind this phenomenon remain unknown.

Main methods: Herein, 10 wk-old B6129SF2/J male mice were exposed to acute ischemia/reperfusion (30minI/24hrsR) injury immediately followed by intracardiac injection of either EphrinA1-Fc or IgG-Fc. After 24 hrs of reperfusion, sections of the infarct margin in the left ventricle were imaged via transmission electron microscopy, and mitochondrial function was assessed in both permeabilized fibers and isolated mitochondria, to examine mitochondrial structure, function, and energetics in the early stages of repair.

Key findings: At a structural level, EphrinA1-Fc administration prevented the I/R-induced loss of sarcomere alignment and mitochondrial organization along the Z disks, as well as disorganization of the cristae and loss of inter-mitochondrial junctions. With respect to bioenergetics, loss of respiratory function induced by I/R was prevented by EphrinA1-Fc. Preservation of cardiac bioenergetics was not due to changes in mitochondrial JH_2O_2 emitting potential, membrane potential, ADP affinity, efficiency of ATP production, or activity of the main dehydrogenase enzymes, suggesting that EphrinA1-Fc indirectly maintains respiratory function via preservation of the mitochondrial network. Moreover, these protective effects were lost in isolated mitochondria, further emphasizing the importance of the intact cardiomyocyte ultrastructure in mitochondrial dynamics.

Significance: Collectively, these data suggest that intracardiac injection of EphrinA1-Fc protects cardiac function by preserving cardiomyocyte structure and mitochondrial bioenergetics, thus emerging as a potential therapeutic strategy in I/R injury.

Key words: myocardial infarction, ephrinA1, mitochondrial bioenergetics, cardioprotection

Introduction

Cardiovascular disease remains the number one cause of death in the US, accounting for 1 in 3 deaths annually. Heart attacks occur at a rate of one every 40 seconds and incur over $12 billion in health care expenses alone [1]. The epidemiologic, financial, and social burden associated with acute and chronic heart conditions, compounded by a growing aged population and numerous co-morbidities, continues to intensify the prevalence of heart disease as a substantial public health problem. Reperfusion is strictly necessary to rescue the ischemic myocardium, but it is widely known that reperfusion *per se* is causative of further damage [2], which ultimately affects the prognosis of patients who have survived myocardial infarction [3]. Despite the significant advances in basic research made over the last 40 years, treatments that can effectively reduce acute ischemic injury have yet to successfully reach the clinical realm.

Mitochondrial function has been increasingly recognized as a key factor in cardiovascular disease and myocardial infarction [4, 5]. Several, if not all, of the molecular changes that elicit cardioprotection and/or occur after an ischemic insult converge in the mitochondria [6]. Manipulation of the metabolic profile of cardiomyocytes during ischemia/reperfusion (I/R) injury is currently being explored as a potential strategy for mitigation of tissue injury [7]. However, controversy exists in the field as to the role and relative contribution of different aspects of mitochondrial function during I/R injury, including alterations in substrate utilization, electron transport, calcium handling, and oxidative stress [4, 8, 9]. Nonetheless, recent findings on the spatio-temporal organization of the mitochondria in cardiomyocytes supports the notion that the maintenance of the electrical “power grid” that conforms the mitochondrial network is a key determinant of the cardiomyocyte’s capacity to endure an ischemic insult [10]. Consequently, mitochondrial-targeted therapies are currently being developed to treat ischemic heart disease and cardiomyopathy [11].

EphrinA1, a highly-conserved membrane-anchored receptor tyrosine kinase ligand expressed in healthy murine as well as human cardiomyocytes, is lost following an ischemic event [12-14]. Previous work from our group has shown that intracardiac injection of its recombinant form (EphrinA1-Fc) at the time of coronary artery ligation in mice reduces infarct size, cardiomyocyte apoptosis, and inflammation in both acute ischemia/reperfused [13] and chronically non-reperfused [12] myocardium. Specifically, in acute I/R we observed 46% reduction in infarct size,

complete preservation of cardiac function, and changes in metabolic protein levels that suggested improved ischemic tolerance however, the specific cellular alterations behind these rescue effects remain unknown [13]. The ability of a terminally differentiated cardiomyocyte to withstand an ischemic insult is inextricably linked to energetics and cellular ultrastructure [15]. With the combination of electron microscopy imaging and high-resolution mitochondrial respirometry, the present work comprises a thorough mitochondrial phenotyping study to assess the impact of ephrinA1-Fc (EA1) intramyocardial administration on cardiomyocyte bioenergetics in the context of acute I/R injury.

Methods

Animals and Ethical Statement. All animal research protocols were approved by the East Carolina University Institutional Animal Care and Use Committee (IACUC) following the guidelines of the National Institutes of Health for the Care and Use of Laboratory Animals. The Department of Comparative Medicine at The Brody School of Medicine, East Carolina University, maintained animal care. 10-week old, male B6129SF2/J mice purchased from The Jackson Laboratory (stock #101045) were housed in a temperature-controlled (22 ºC) facility with a 12 hr light/dark cycle, and free access to food (standard chow diet) and water. Mice were randomized to a *sham*-operated control group (CTL; n=17), or acute ischemic injury followed by reperfusion containing either IgG-Fc (n=21; 110-HG, R&D) or EphrinA1-Fc (n=18; Sigma, E9902) (I/R and I/R+EA1, respectively). To perform the thoracotomy, mice were anesthetized with an intraperitoneal injection of Avertin (20 mg/Kg BW) and mechanically ventilated with 95% O_2/5% CO_2. Acute ischemic injury was induced by a 30 min occlusion of the left anterior descending coronary artery (LAD). Ischemia was confirmed by visible blanching of the tissue distal to the occlusion. Ligation was immediately followed by intracardiac injection of 6µg/6µL EphrinA1-Fc or IgG-Fc into the infarct margin (border between healthy, pink tissue and the ischemic region as evidenced by tissue pallor), as previously described and shown (https://www.jove.com/video/2581/coronary-artery-ligation-intramyocardial-injection-murine-model) [16]. Briefly, this was done using a Hamilton syringe with a 30gauge beveled sterile needle which was inserted into the anterior wall at an angle of approximately 15° above and to the right (toward the right ventricle) of the ligation, advanced into the infarct margin (approx. 3mm; please refer Fig 3 in JoVE protocol link above and Dries et al. 2011, Fig 1), and slowly withdrawn after the injection to minimize extrusion of the injectate that occurs as a consequence of contraction [16]. After closing the ribcage and muscle, administration of 1-3 drops of 0.25% marcaine 1:10 in

sterile saline to the muscle, and suturing the skin, mice were housed in a warm chamber until they recovered sternal recumbency and returned to the vivarium. We have previously found that that the injection does not cause notable injury and the injectate is washed out after 4 hours so, to save on animals and reagents, we did not do additional in vivo studies with IgG-Fc and ephrinA1-Fc injection without I/R. After 20-24 hrs of reperfusion, conscious animals underwent echocardiographic assessment and were subsequently anesthetized with euthasol (100 mg/Kg BW) and after ensuring adequate sedation with negative response to toe-pinch, the thoracic cavity was opened to remove the heart. Heart sections were allocated to the respective assays as shown in Figure 1. Isolated mitochondria or permeabilized cardiac muscle fibers were obtained from section #2 from the left ventricle (Figure 1) to assess parameters of mitochondrial structure, function, and energetics. No mice died but 2 mice in the IgG-Fc group were excluded due to HR below 400BPM.

Echocardiography and strain analyses. Mice were conscious and gently restrained in prone position on a plexiglass board using elastic cord and wire loops on each limb. Using an MX400 22-55MHz linear-array transducer (Vevo 3100 Imaging System, VisualSonics, Toronto, Canada), standard short- and long-axis views were obtained at the mid-papillary level in both M- and B-mode at >200 frames/second [17, 13, 18]. Image analysis was performed offline using a speckle-tracking algorithm provided by VisualSonics (VevoStrain, VisualSonics). Echocardiographic images showing the parasternal long axis view (PSLAX) were used to obtain LS and GLS measurements. Three cycles of successive R-waves were selected for speckle tracking. Four endocardial points were selected on the echo in a frame between systole and diastole. Acquisition and analyses were performed blindly by the same trained investigator. No differences in heart rate (HR) were observed.

Fixation. Hearts were cut into 2-3 mm^2 cubic pieces using a sharp scalpel and fixed overnight in 3 % glutaraldehyde and then post-fixed for one hour in 1 % osmium tetroxide (Stevens Metallurgical) [19]. Tissues were then dehydrated by passage through an ethanol series (25, 50, 75, 95 and 100 %, 15 min each) and embedded in increasing concentrations of Spurr media in ethanol (30 % for 30 min, 70 % one hr, 100 % for 2 hrs, 100 % for 30 min). Tissues were cut into ultrathin sections (70 nm) and placed on fresh plasma-etched 200hexagon mesh copper grids (Electron Microscopy Science).

Transmission electron microscopy. Sections were examined in a 1200 EX transmission electron microscope (JEOL) at 80-kV accelerating voltage, and images were recorded using an EMSIS MegaView G3 charge-coupled device digital camera (Munster, Germany) [19]. Approximately nine images were collected at x10,000 to maximize coverage of broader region from each mouse (n = 3 mice/group), with each EM image depicting 24-78 mitochondria (average 62; total ~500/mouse heart). Mitochondrial two-dimensional morphology parameters were determined manually using ImageJ software as previously described [20]: 1) Mitochondrial size is reported as surface area in squared micrometers, 2) mitochondrial external perimeter in micrometers, 3) the aspect ratio (AR) represents the length-to-width ratio and is calculated as [major axis/minor axis] in arbitrary units, 4) the form factor (FF) reflects the branching aspect of mitochondria and is calculated as (external perimeter^2)/(4π*surface area)] in arbitrary units, 5) circularity and roundness, computed as 4$\pi\cdot$(surface area/perimeter^2) and (4*surface area)/(π*major axis^2) respectively, comprise measures of sphericity, where values of 1 resemble perfect spheroids in arbitrary units. The number of electron-dense inter-mitochondrial junctions (IMJs) was determined as in [21], as well as the number of lipid droplets.

Western Blotting. Whole left ventricles previously stored in -80 ºC were homogenized in Protein Extraction Reagent Type 4 (Sigma C0356), supplemented with protease inhibitor (ThermoFisher A32953) for detection of several proteins by Western blotting. Primary antibodies utilized were SERCA2 ATPase (ThermoFisher, cat. #MA3-919), GRP78/ HSPA5 (ThermoFisher, cat. #PA1-16857), Beclin1 (Thermofisher, cat. #PA1-16857), ChChd3 (Thermofisher, cat. #PA 5-31578), Mfn1 (ThermoFisher, cat. #PA5-38042), OPA1 (ThermoFisher, cat. #PA1-16991), Fis1 (PA 1-41082), Drp1 (PA5-34768), EphrinA1 (SantaCruz Biotechnology, cat #Sc-911), GAPDH (Cell Signaling, cat #2118), alpha tubulin (Invitrogen, cat. #138000), and phospho-alpha tubulin (Tyr272) (ThermoFisher, cat. #PA5-37831). Membranes were blotted using either mouse IgG-Fc secondary antibody (Thermo scientific cat. #31455) or rabbit IgG HRP-conjugated antibody (R&D systems cat. #HAF008), and the chemiluminescent substrate SuperSignal West Pico PLUS (ThermoFisher, cat. #34078), and imaged in a ChemiDoc-ItTS2 810 Imager, UVP.

Permeabilized muscle fiber bundle (PmFB) preparation. A section of the left ventricular free wall was dissected and immediately placed in ice-cold buffer X (50 mM K-MES, 35 mM KCl, 7.23 mM K_2EGTA, 2.77 mM CaK_2EGTA, 20 mM imidazole, 20 mM taurine, 5.7 mM ATP, 14.3 mM phosphocreatine, and 6.56 mM $MgCl_2$-6H2O, pH=7.1)

for mechanical separation with fine forceps under a dissecting microscope as described elsewhere [22]. Separated LV fiber bundles were incubated in buffer X containing 30 µg/mL saponin, for 30 min at 4 °C, and then transferred to buffer Z (105 mM K-MES, 30 mM KCl, 1mM EGTA, 10 mM K_2HPO_4, 5 mM $MgCl_2$-6H2O, 0.5 mg/mL BSA, pH=7.1) at 4 ºC for 15 min. At the conclusion of respiratory assessment, fibers were rinsed in dH_2O and freeze-dried (typical dry weight 0.1 - 0.2 mg).

Mitochondrial respiratory capacity (JO_2) and JH_2O_2 emitting potential. Respiratory capacity in PmFBs or isolated mitochondria from LV was measured by high-resolution respirometry (O2K, OROBOROS Innsbruck, Austria), in buffer Z supplemented with 20 mM creatine monohydrate and 10 µM blebbistatin, at 37 ºC to inhibit myosin II. To assess lipid and Krebs cycle intermediates-supported respiration, substrates were sequentially added in the following concentrations: 18 µM Palmitoyl-carnitine, 5 mM L-carnitine, 0.5 mM malate, 4 mM ADP, 10 mM pyruvate, 10 mM glutamate, 10 mM succinate. For experiments using isolated mitochondria, 25 µg of total mitochondrial protein was used. JH_2O_2 was measured using the Amplex UltraRed/Horseradish Peroxidase fluorescence system in buffer Z supplemented with 10 µM Amplex UltraRed (Invitrogen), 1 U/mL horseradish peroxidase, 20 U/mL CuZn superoxide dismutase, and 10 µM Blebbistatin. Data was collected in a Fluorolog spectrofluorometer (HORIBA Jobin Yvon), at 37 ºC. 10 mM succinate or 18 µM palmitoyl-carnitine + 5 mM L-carnitine was added followed by 1 µM 1,3-bis(2-chloroethyl)-1-nitrosourea (BCNU), 1 µM auranofin.

Determination of the mitochondrial thermodynamic force-flow relationship. As initially described by B. Glancy, et al. and successfully implemented by others [23, 24], intermediate steady-state rates of JO_2 were measured at different levels of metabolic demand (ATP/ADP ratio) using a progressive creatine kinase (CK) clamp, at 37 ºC. With known concentrations of creatine, phosphocreatine, ATP, and the CK equilibrium constant, the ATP/ADP ratio and therefore the free energy of ATP hydrolysis (ΔG_{ATP}) can be calculated from: $\Delta G_{ATP} = \Delta G_{ATP}° - 2.3$ RT*K*2.3*log[([PCr]K_{CK})/[Cr][Pi])], where $\Delta G_{ATP}°$ is the standard ΔG_{ATP} (−7.592 kcal/mol), R is the gas constant (1.987 cal K^{-1} mol^{-1}), and T is the temperature (310 K) [23]. Mitochondrial respiration in state 4 conditions (no ADP) was supported by 18 µM palmityl-carnitine, 5 mM carnitine, 5 mM pyruvate, and 2.5 mM malate, in the presence of 10 U/mL CK, 1.5 mM PCr, 5 mM Cr, and 5 mM ATP. Subsequent additions of PCr (2.75, 5.25, 10, 20, 35 and 45 mM) progressively shifted the CK equilibrium, increasing the ATP/ADP ratio and thus lowering

192 respiration. Steady state JO_2 was determined at each PCr concentration, from which ΔG_{ATP} and [ADP] were
193 calculated.
194 *Citrate synthase activity.* Freeze-dried PmFBs utilized for JO_2 measurements were homogenized in CelLytic lysis
195 buffer (Sigma #C3228) and citrate synthase activity was measured using the kit (Sigma #CS0720).
196 *Mitochondrial isolation.* Sections of the left ventricle were harvested and immediately homogenized in
197 mitochondrial isolation media (0.3 M sucrose, 10 mM HEPES, 1 mM EGTA) containing 1 mg/mL BSA, on ice
198 [25]. Due to the limited amount of tissue available, isolated mitochondria from LV slices of two mice were pooled
199 together for each sample. Homogenates were spun at 800 G/ 10 min/ 4 ºC, and the supernatant was spun again at
200 1,200 G/ 10 min/ 4 ºC. The pellet was re-suspended in mitochondrial isolation media (no BSA) for a last
201 centrifugation step (1,200 G/10 min/4 ºC). The final pellet was re-suspended in 100 µL mitochondrial isolation
202 medium, and protein quantification was assessed using the Pierce BCA Protein Assay Kit (Thermo Fisher #23225).
203
204 *Measurement of real-time mitochondrial JO_2 and JATP.* As previously described, ATP production was followed via
205 the 1:1 stoichiometry with $NADP^+$ reduction from the glucose/hexokinase/glucose-phosphate dehydrogenase
206 enzymatic clamp [26]. The system contained 1 U/mL hexokinase, 2.5 mM glucose, 5 U/mL mM glucose-phosphate
207 dehydrogenase (G6PDH), 2.5 mM $NADP^+$, and added isolated mitochondria at 5 µg/mL in buffer Z (+5 mg/mL
208 BSA, 1 mM EGTA, 20 mM creatine), at 37 ºC. 0.2 mM Ap5A (P1,P5-di(adenosine-5′)pentaphosphate) was added to
209 inhibit adenylate kinase as an alternative non-OXPHOS source of ATP synthesis. Respiration was supported by 5
210 mM pyruvate, 5 mM glutamate, 5 mM succinate, and 0.5 mM malate. NADPH was measured by autofluorescence
211 (λ_{ex} = 340, λ_{em} = 460) simultaneously with O_2 consumption using a customized system integrating fluorescence
212 (FluoroMax-3; Horiba Jobin Yvon, Edison, NJ) with high-resolution respirometry (Oroboros Oxygraph-2k,
213 Innsbruck, Austria) via a fiber optic cable (Fiberguide Industries). Rates of ATP synthesis (*J*ATP) were quantified
214 using an ATP titration standard curve generated in the presence of the enzyme-coupled system and substrates but no
215 mitochondria. Steady-state OXPHOS flux rates (JO_2 and *J*ATP) were determined after sequential additions of ADP:
216 20 and 200 µM.
217
218 *Mitochondrial membrane potential*. $\Delta\Psi$ and JO_2 rates were measured simultaneously as previously described [27],
219 using the Oroboros Oxygraph-2k combined with electrodes sensitive to the membrane potential-dependent probe

tetraphenylphosponium (TPP+) and O_2, at 37 ºC. Fresh isolated mitochondria from LV was added at a concentration of 50 µg protein/mL in the chamber. All experiments were run in buffer Z supplemented with 1 mM EGTA and 20 mM creatine, in the presence of 1.5 µM carboxyatractyloside, 5 µM rotenone, 0.5 mM GDP, and 10 mM succinate. The TPP electrode was calibrated by a 6-point titration (1.1-1.6 µM TPP^+) at the beginning of each experiment. Membrane potential was progressively decreased by the titration of malonate (complex II inhibitor) from 0.1 to 7.5 mM. $\Delta\Psi$ was calculated from the Nernst equation based on the distribution of TPP^+ [27].

Activity of dehydrogenase enzymes. Pyruvate dehydrogenase (PDH), AKG dehydrogenase (AKGDH), branched chain ketoacid dehydrogenase (BCKDH), NAD-linked Isocitrate DH (ID3), malate dehydrogenase (MDH2), glutamate dehydrogenase (GDH), trifunctional protein of beta oxidation (HADHA), NADP-linked isocitrate dehydrogenase (IDH2) and malic enzyme (ME) were determined by kinetic studies in LV homogenates [24].

Metabolite analyses. Briefly, sections of the apical region of the left ventricle just below the suture were cut free (Figure 1), blotted, and frozen in an aluminum clamp cooled in liquid nitrogen. While frozen, sections were quickly weighed to allow normalization of metabolites to tissue mass. Nucleotides levels were determined in cardiac tissue extracts by rapid and sensitive ultra-performance liquid chromatography as previously described [28]. Briefly, slices of the left ventricle (Figure 1A) were flash-frozen in liquid nitrogen and weighed. Metabolites were extracted in 20-30 -fold excess ice-cold 0.5 N perchloric acid supplemented with 5mM EDTA with rapid glass-on-glass homogenization. Extracts were neutralized and perchlorate was removed by addition of ice-cold 1N KOH and subsequent centrifugation at 4°C. Concentrations of adenine nucleotides (ATP, ADP, and AMP), and adenine nucleotide degradation products (IMP, adenosine, adenine), as well as guanosine nucleotides (GTP) were determined by UPLC using a Waters Acquity UPLC H-class system as in [28].

Statistics. Data are presented as means ± SEM. Statistical analysis were performed with one-way ANOVA, followed by Sidak's multiple comparisons test (* vs. CTL, and # vs. I/R). Graph Pad Prism 7 was used for statistical analysis and data presentation. Statistical significance was set at a P value of ≤ 0.05.

Results

EphrinA1-Fc administration during acute I/R helps preserve cardiac function.

Mice were randomized to a *sham*-operated control group (*sham*), or acute ischemic injury induced by ligation of the left anterior descending coronary artery immediately followed by intramyocardial injection of 6µg/6µL of either IgG-Fc (I/R) or EphrinA1-Fc (I/R+EA1) with a sterile 30 gauge Hamilton syringe [16]. After a 30 min occlusion, the ligature was released to reperfuse the heart, the thoracic cavity was closed, and following recovery, the animals were returned to the vivarium. At 24 hrs post-injury and before sacrifice, global cardiac function and strain was assessed using M-mode and B-mode echocardiography (Table 1). In keeping with previously reported findings from our group [13], EA1 treatment significantly improved ejection fraction (+46%, ***p<0.0005) and fractional shortening (+49%, ***p< 0.0005) compared to I/R + IgG-Fc. Longitudinal strain rate (LS) and global longitudinal strain were significantly decreased with I/R (-76%, **p<0.005 vs *sham; -71% ***p<0.0005 vs sham*), but preserved by EA1 (-76%, ## p<0.005 and +45%, *p<0.05 vs I/R).No differences in heart rate (HR) were observed but cardiac index (CI; ml/min/g) was decreased in the I/R + IgG-Fc group compared to control and EA1 due to decreased stroke volume. Administration of EA1 thus preserves cardiac function during the critical stages of early repair (24 hrs post-I/R).

Table 1. **EphrinA1 administration in I/R preserves cardiac function.** Echocardiographic measures of LV function and remodeling: ejection fraction, EF %, fractional shortening, FS %, heart rate, HR, cardiac index, CI, longitudinal strain rate, LS, and global longitudinal strain, GLS %. Data are expressed as means +/- SEM. * p<0.05, **p<0.005 and ***<0.0005 vs *sham* and # p<0.05, ## p<0.005 vs I/R from one-way ANOVA analysis. N = 3-4 mice/group.

Group	EF (%)	FS (%)	HR	CI	LS	GLS
control	89 ± 4.5	59 ± 2.7	588 ±20	0.74 ± 0.07	-21.6 ± 3.2	-38 ± 7.3
I/R + IgG-Fc	45 ± 9.7***	27 ± 5.1***	591 ± 33	0.43 ± 0.11**	-4.8 ± 1.9**	-11.4 ± 5.7***
I/R + ephrinA1-Fc	84.3 ± 1$^{###}$	53 ± 4.6**	604 ± 23	0.67 ± 0.09	-20 ± 5.8$^{##}$	-21 ± 3.6*

Figure 1.

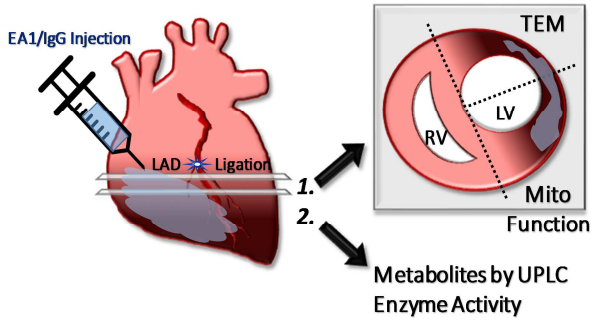

At sacrifice, hearts were collected and specific sections with respect to the ligature were allocated to the designated experimental endpoints (depicted in Figure 1). In a separate cohort of mice, whole left ventricle homogenates were used for western blotting. Unlike in previous observations of longer I/R periods [12, 29], there was no reduction of EA1 protein levels in the present model of acute I/R injury (Figure 2A), despite a subtle reduction in gene expression (data not shown). Protein levels of sarco/endoplasmic reticulum Ca^{2+} adenosine triphosphatase-2a SERCA2a, a cornerstone protein for calcium homeostasis during the cardiac cycle [30] normally decreased in acute ischemia and chronic heart failure [31-34], was 49% ($p<0.05$) higher in I/R+EA1 compared to I/R (Figure 2B), likely contributing to preserved contractile function and mitigation of deleterious calcium overload. ChChd3, an abundant scaffolding protein localized in the inner mitochondrial membrane that stabilizes protein complexes to help maintain crista integrity and thus mitochondrial function [35], was 54% higher ($p<0.05$) with EA1 administration (Figure 2C) compared to I/R. Expression of GRP78, a master chaperone sensor of ER stress and modulator of the apoptotic response [36]), was two-fold higher with I/R ($p<0.0005$) (Figure 2D), whilst unchanged with EA1 administration relative to *sham*, at a remarkable 60% lower value ($p<0.005$) than their I/R counterparts. Furthermore, Beclin-1, a protein that plays a central role in cardiomyocyte autophagy and apoptosis [37, 38], was increased by 20% ($p<0.05$) with administration of EA1 relative to I/R (Figure 4A). These findings support previous reports on the efficiency of EA1 to reduce to cardiomyocyte damage and reduce infarct size [12, 13].

Figure 2.

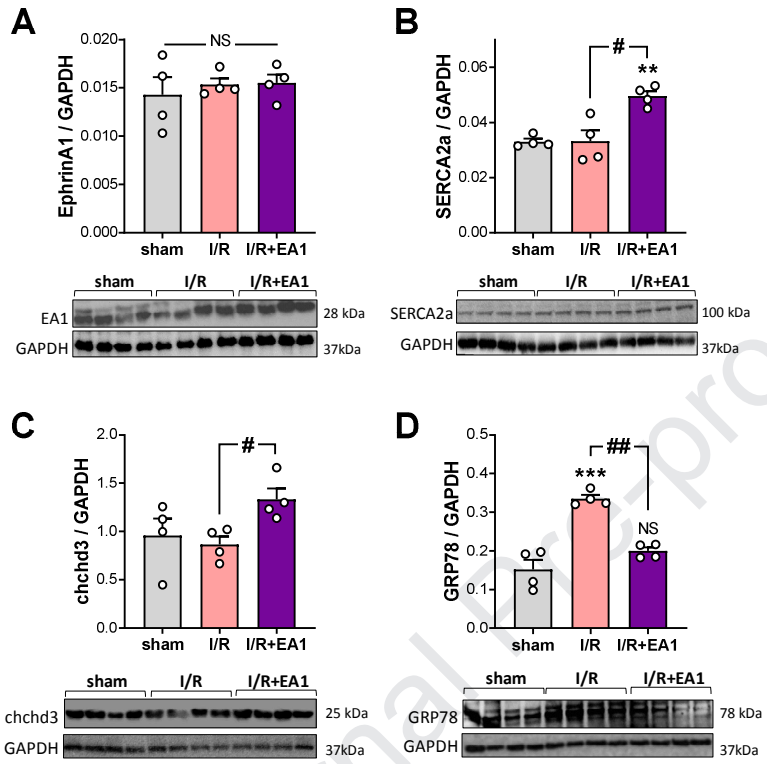

EphrinA1-Fc administration preserves cardiomyocyte and mitochondrial ultra-structure in acute I/R.

Sections of the left ventricular infarct margin (Figure 1) were imaged by transmission electron microscopy (TEM). Representative TEM images are shown in Figure 3. In agreement with previous reports of altered mitochondrial morphology with heart failure [39-41], the present model of acute I/R significantly altered mitochondrial organization and overall cellular ultra-structure (Figure 3A-C). Qualitatively, administration of EA1 seemed to

306

307 **Figure 3.**

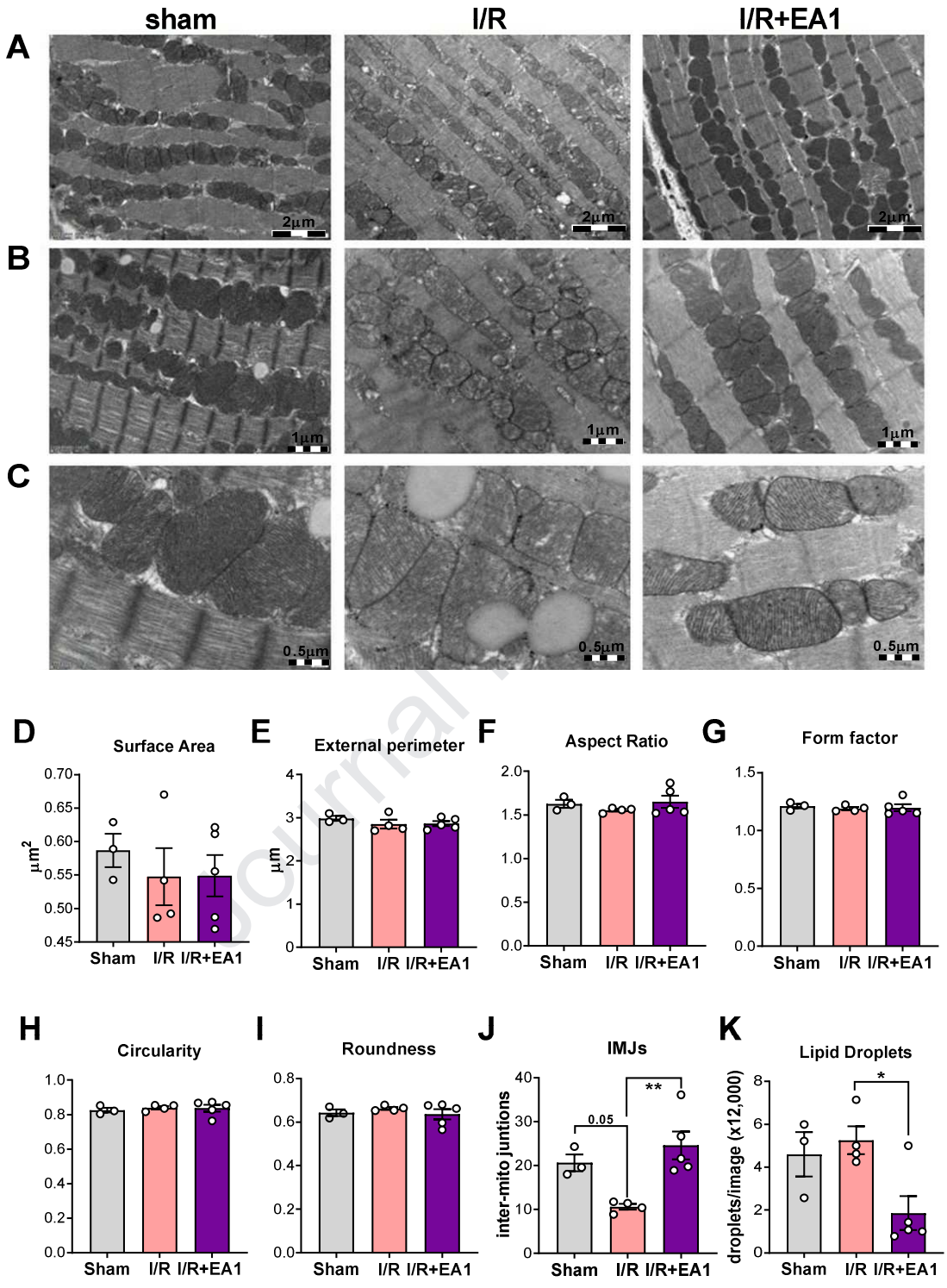

prevent the sarcomere and mitochondrial disorganization, and loss of Z-lines alignment (Figure 3A-C). Mitochondrial two-dimensional morphological parameters including surface area, perimeter, aspect ratio, form factor, and sphericity were quantified (Figure 3D-I). Although no statistical differences were detected, qualitatively, overall spatial organization of mitochondria in EA1-treated mice appeared more comparable to the *sham* mice than the I/R group. In addition, electron-dense inter-mitochondrial junctions presented trending lower values with I/R ($p=0.05$ vs *sham*) that was reversed with EA1 administration ($p=0.005$ vs I/R) (Figure 3J), and lipid droplet number were reduced in a I/R vs I/R+EA1 comparison ($p<0.05$) (Figure 3K).

Evaluation of EphrinA1-Fc-mediated effects in mitochondrial dynamics.

Mitochondrial morphology is highly dynamic and finely regulated by several key players that orchestrate fission, fusion and mitophagy processes. Mitochondrial dynamics play a key role in heart failure [42]. Figure 4 shows western blot analysis of some of the main regulators of fission (such as Drp1 and Fis1), and fusion (OPA1 and Mfn1). In rat, it has been shown that high LAD ligation only decreases OPA1 expression levels, while in human ischemic cardiomyopathy OPA1 has been reportedly decreased with Mfn1/2 and Drp1 levels increased [43]. In the present model of acute I/R injury in mice, none of these proteins were changed in an I/R vs *sham* comparison, but EA1 administration significantly increased levels of Drp1 (+22%, $p<0.05$) and Fis1 (34%, $p<0.05$) (Figure 4B-C), and decreased Mfn1 levels (-51%, $p<0.05$) (Figure 4E) relative to the I/R group. There were no differences in OPA1 levels across all three groups (Figure 4D).

Figure 4.

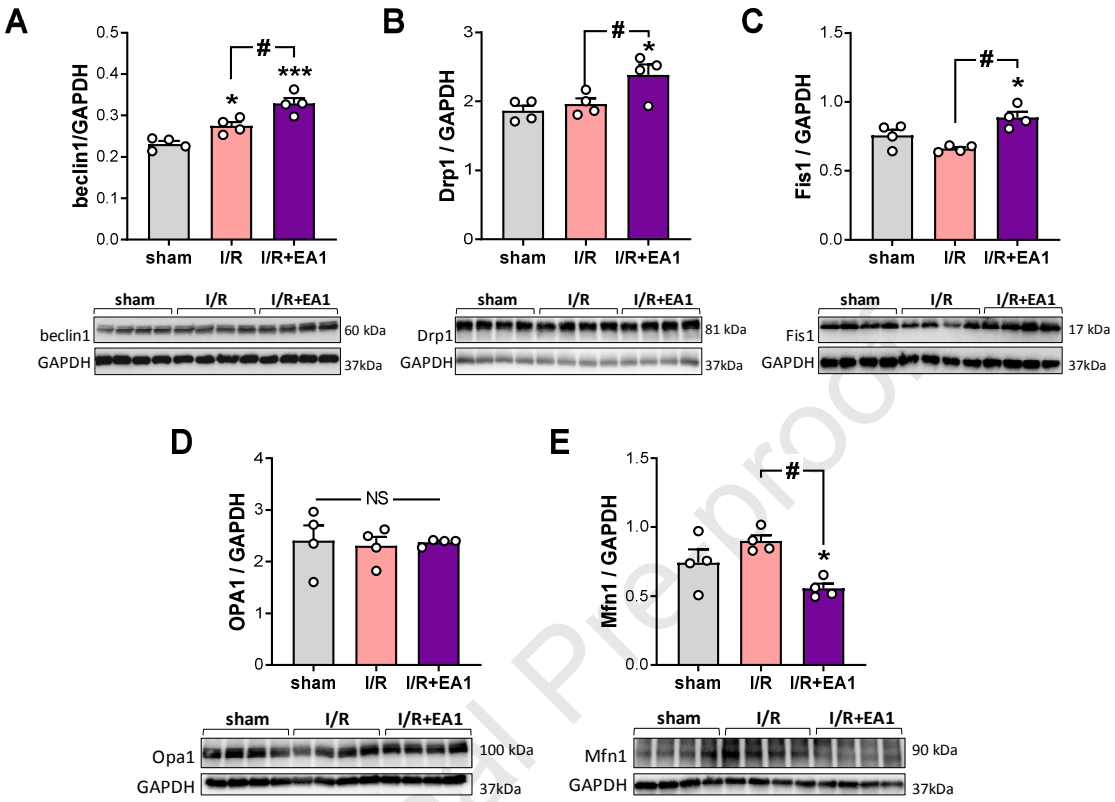

EphrinA1-Fc administration in I/R preserves mitochondrial respiratory capacity independent of changes in H_2O_2 emitting potential.

Mitochondrial function plays a key role in I/R [4, 5]. To determine the effects of EA1 administration on different parameters of mitochondrial function such as mitochondrial respiratory capacity (JO_2) and H_2O_2 emitting potential (JH_2O_2), permeabilized cardiac muscle fibers (PmFBs) were prepared from a section of the LV infarct margin (Figure 1). Respiration supported by lipid substrates (palmitoyl-carnitine) and malate was not affected by I/R +/- EA1, in state 4 (no ADP) or 3 (+ADP) conditions. However, subsequent addition of pyruvate, glutamate and succinate revealed a 30% decrease ($p<0.005$) in state 3 JO_2 with I/R, which was preserved by EA1 administration (Figure 5A). Of note, addition of 0.1 µg/mL EA1 directly into the O2K chamber, a concentration well above the one used for intramyocardial injections *in vivo* did not affect JO_2 acutely (data not shown). Interestingly, no changes in JH_2O_2 emitting potential were detected in I/R +/- EA1 relative to the *sham* group, using either palmitoyl-carnitine + carnitine (Figure 5B, left panel), or succinate (Figure 5B, right panel) as substrates, and in the presence or absence of

351 the antioxidant buffering system (+BCNU/AF, specific inhibitors of glutathione and thioredoxin reductases).
352 Importantly, mitochondrial content evaluated by citrate synthase activity [44] in homogenates of the same PmFBs
353 utilized for JO_2 experiments revealed no differences among groups (Figure 5C). This suggests that the cellular
354 alterations behind the loss and preservation of mitochondrial respiratory capacity with I/R and EA1 respectively,
355 may not be mediated by changes in mitochondrial content or the potential for electron leak/ROS generation.

356 **Figure 5.**

357

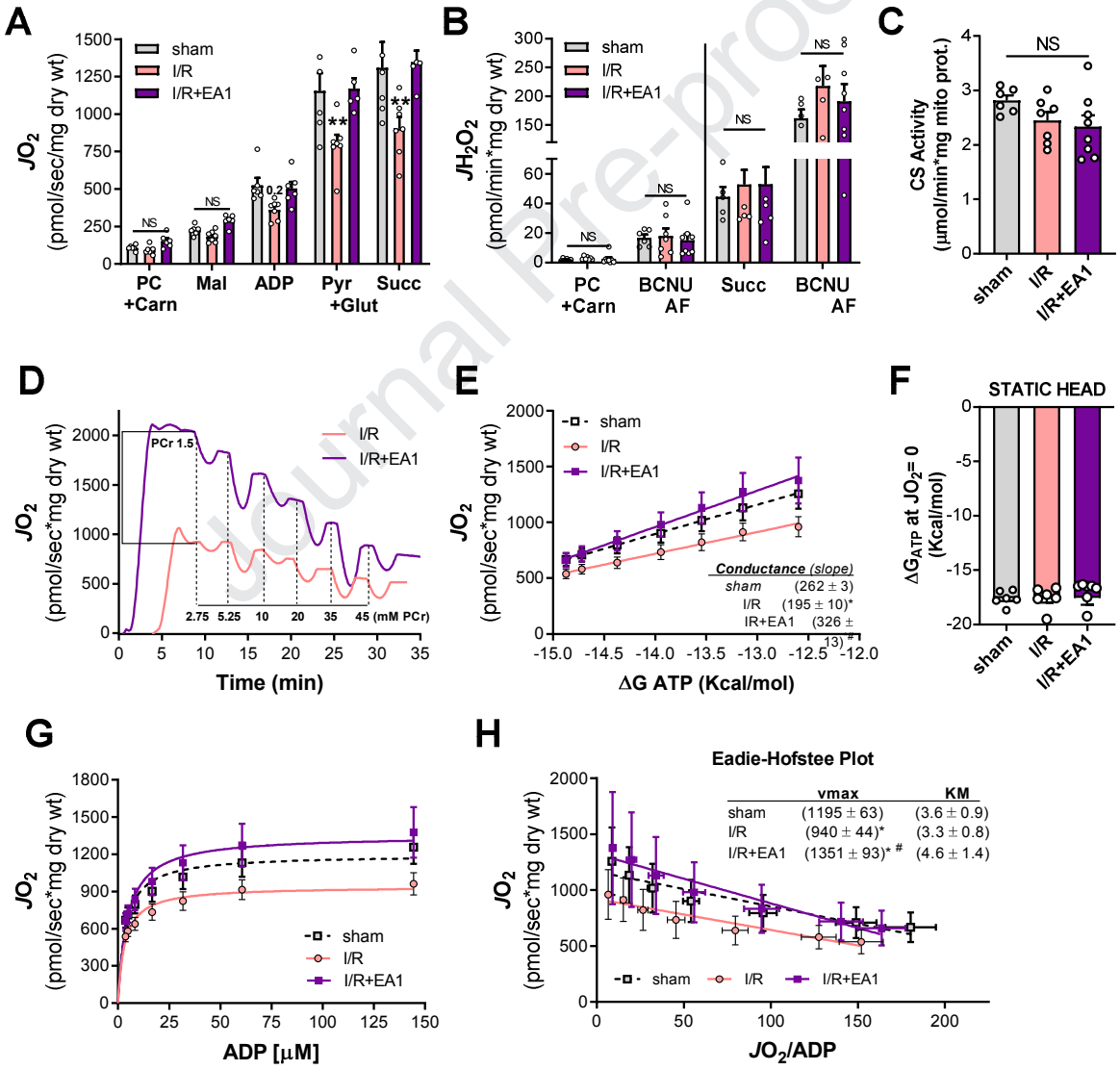

358
359

EphrinA1-Fc administration in I/R preserves mitochondrial respiratory control under physiological thermodynamic constraints.

To gather further insight into the effects of EA1 on mitochondrial function with I/R, sub-maximal steady-state rates of JO_2 were measured at different levels of metabolic demand (ATP/ADP ratio), using a progressive creatine kinase (CK) energy clamp as [24, 23]. Briefly, using CK in large excess and known added amounts of creatine, phosphocreatine, and ATP, the extra-mitochondrial ATP/ADP ratio can be manipulated, re-setting the steady-state JO_2 with each addition of PCr. Representative traces of the experiment for the I/R and I/R+EA1 groups are shown in Figure 5D. Each PCr addition shifts the CK equilibrium increasing the ATP/ADP ratio, and therefore the free energy available from ATP hydrolysis (ΔG_{ATP}), which can be calculated as described in the methods. Figure 5E shows the JO_2 vs ΔG_{ATP} plot, from which the line intersection at the *x* axis represents the "static head" of the system (most negative ΔG_{ATP} when respiration is zero), and the slope comprises a measure of the overall "conductance" of the electron transport system (ETS, OXPHOS and ATPase fluxes [24, 23]), an indicator of how well the system can adjust and respond to different levels of metabolic demand. While values of static head ΔG_{ATP} were unchanged (Figure 5F), overall conductance (slopes reported in Figure 5E) was decreased by 25% with I/R ($p<0.05$), but preserved with EA1 administration (+124%, $p<0.05$).

Given that no differences were found in JH_2O_2 emitting potential (Figure 5B) or static head ΔG_{ATP} [45], the possibility of EA1 minimizing ROS emitting potential the main driving cellular change for increased conductance seems unlikely. Hence, it was hypothesized that EA1 exerts mainly a kinetic protective effect in mitochondrial function, increasing OXPHOS conductance. To determine whether the improved force-flow relation was due to changes in sensitivity to ADP, ADP kinetics were analyzed (Figure 5G-H). Figure 5H shows secondary analysis of Figure 5G, using the Eadie-Hofstee plot where $y = -(KM_{ADP})x + Vmax$. The apparent KM for ADP remained unchanged across all three groups. However, Vmax was 21% lower with I/R ($p<0.05$), and 113% higher ($p<0.05$) with EA1 administration. The lack of changes in mitochondrial content (Figure 5C) suggests that the consistently higher JO_2 rates observed with EA1 administration across different levels of metabolic demand were the result of an increase in conductance, and not due to changes in ADP affinity or mitochondrial content. This is suggestive of EA1 exerting protection in OXPHOS kinetics, likely through preservation of mitochondrial structure and organization.

388 *EphrinA1-Fc increases OXPHOS conductance without altering dehydrogenase activity, membrane potential or ATP*
389 *synthesis.*

390 From a kinetic perspective, many parameters could contribute to the enhanced OXPHOS conductance observed with
391 EA1 administration, such as activity of the dehydrogenase enzymes, any of the step-wise kinetic steps in the ETC,
392 membrane potential (ΔΨ), and the rate of ATP synthesis [23]. To determine whether EA1 directly affects any of
393 these parameters, mitochondria were isolated from LV for further functional assessment.

394

395 The activity of pyruvate dehydrogenase (PDH), AKG dehydrogenase (AKGDH), branched chain ketoacid
396 dehydrogenase (BCKDH), NAD-linked Isocitrate DH (ID3), malate dehydrogenase (MDH2), glutamate
397 dehydrogenase (GDH), trifunctional protein of beta oxidation (HADHA), as well as the NADP-linked isocitrate
398 dehydrogenase (IDH2) were determined in whole LV homogenates. Activities of MDH2, IDH3 and HADHA were
399 not significantly affected by I/R +/- EA1. PDH, AKGDH, and GDH were downregulated with I/R compared to *sham*
400 (- 35-45%, $p<0.05$), but the effect was not reversed by EA1 administration (Figure 6A), suggesting that the
401 preservation of bioenergetics mediated by EA1 does not involve the dehydrogenase enzymes.

402 **Figure 6.**

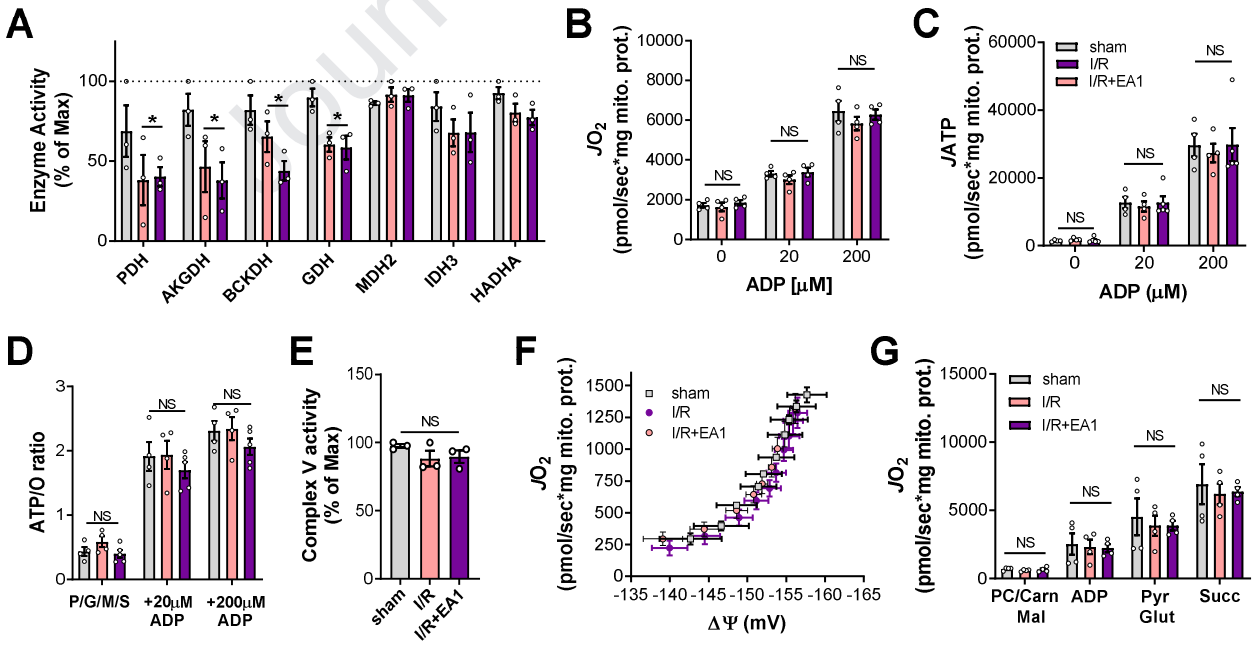

403
404

Simultaneous, real-time rates of ATP production (*J*ATP) and O_2 consumption (JO_2) were determined as previously described [26] in isolated mitochondria from LV. Surprisingly, there were no differences in JO_2 (Figure 6B) or *J*ATP (Figure 6C) rates with I/R +/- EA1, in the absence or presence of increasing levels of ADP. Consequently, the efficiency of ATP production (ATP/O ratio) also remained unchanged (Figure 6D). In accordance, no differences were detected in complex V activity (Figure 6E), or mitochondrial membrane potential across a wide range of respiratory states (Figure 6F). Metabolite analysis by UPLC showed unchanged levels of the high-energy metabolites GTP, ATP, ADP as well as their degradation products (IMP, adenosine, adenine) across the three groups (Figure 7) and there was no difference in the calculated energy charge (ATP + ½ ADP/total nucleotides [46]: sham = 0.648 ± 0.015; IgG-Fc = 0.651 ± 0.021; EA1 = 0.665 ± 0.010). Cumulatively, these data indicate that the EA1-mediated preservation of mitochondrial bioenergetics via OXPHOS conductance is absent in the isolated organelle, suggesting a direct link with the mitochondrial network ultra-structure.

435 **Figure 7**

436

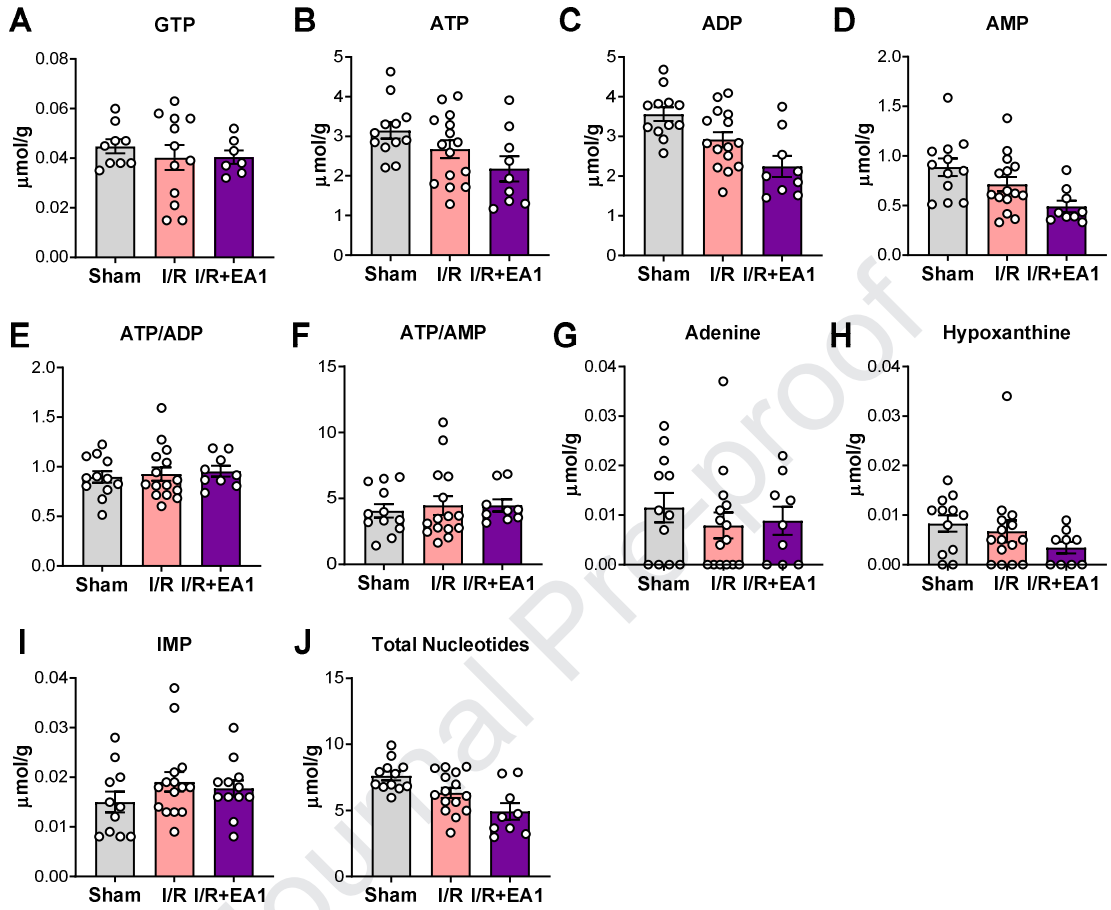

437

438

439 *EphrinA1-Fc-mediated preservation of bioenergetics involves the cytoskeleton, and/or mostly impacts interfibrillar*

440 *mitochondria.*

441 Cytoskeletal structures such as microfilaments and microtubules are known to directly interact with mitochondria,

442 and disruption of the cytoskeleton morphology and myocardial ultrastructure are associated with decreased

443 myocardial function [41]. The main difference between testing mitochondrial respiratory capacity in PmFBs and

444 isolated mitochondria is that, in the former, mitochondria is stripped from all cellular and cytoskeletal components,

445 and the mitochondrial network is completely disassembled into single organelles. Thus, a simple control experiment

446 was to test the same JO_2 protocol utilized in Figure 5A for PmFBs, in isolated mitochondria. As shown in Figure

447 6G, the observed differences in mitochondrial JO_2 disappeared when respiratory function was tested in isolated

mitochondria, suggesting that the protective effects of EA1 are potentially mediated by cytoskeletal components. Because several aspects of mitochondrial dynamics and function are linked to microtubule (MT) dynamics [47-49], we asked whether EA1 activation of Eph tyrosine kinase receptors could potentially affect the phosphorylation status of α-tubulin, the MT protein unit. Interestingly, phosphorylation of α-tubulin at the Tyr272 residue was reduced by I/R (-50%, $p<0.005$), but preserved with EA1 (Figure 8), suggestive of a potential EA1 target.

Figure 8.

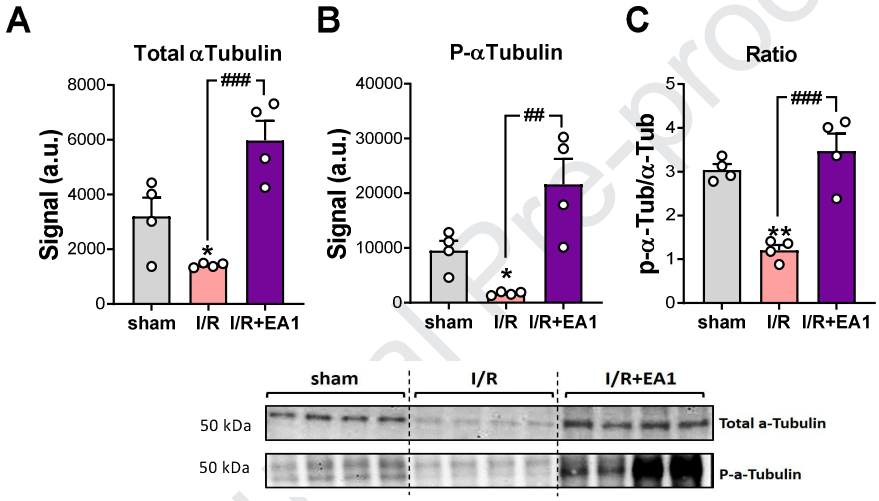

Alternatively, EA1-mediated actions may significantly impact a sub-population of mitochondria within the cardiomyocyte [50]. The mitochondrial isolation procedure used in this study isolates mostly the subsarcolemmal mitochondria, whereas in PmFBs both subsarcolemmal and interfibrillar mitochondrial reticulum are preserved. Both sub-types of mitochondria serve different functions in cardioprotection [51], and interfibrillar mitochondria have been shown to be particularly vulnerable to ischemia [52, 53]. The fact that no differences in respiratory function were observed in the isolated organelle may also be suggestive that EA1-mediated preservation of bioenergetics mostly impacts the interfibrillar mitochondria.

Discussion

EphrinA1 is one of five ligands (A1-A5) that bind and activate nine different Eph-A transmembrane tyrosine kinase receptors (EphA1-A8, and A10). EphrinA1 is localized in the cellular membrane of healthy cardiomyocytes and orchestrates cell positioning and survival, among other functions [54]. Levels of EphrinA1 are decreased in myocardial infarction [12, 13, 29], and previous work from our group has shown that intracardiac injection of its recombinant form, EphrinA1-Fc, at the time of coronary artery ligation in mice reduces infarct size, cardiomyocyte apoptosis, and inflammation in both reperfused [13] and non-reperfused [12] myocardium. The aim of this work was to perform a mitochondrial phenotyping assessment of the early stages of post-I/R injury to explore the cellular changes induced by EphrinA1-Fc that result in preservation of myocardial function. By leveraging a model of acute ischemia/reperfusion injury (30 min/24 hr), herein we: 1) performed measurements of the mitochondrial thermodynamic force-flow relationship for the first time in a model of I/R; and 2) provide evidence that intramyocardial administration of ephrinA1-Fc at the time of coronary artery ligation protects not only cardiomyocyte and mitochondrial network ultrastructure, but also preserves mitochondrial bioenergetics.

Mitochondrial function has been increasingly recognized as a key factor in cardiovascular disease and myocardial infarction [4, 5]. In heart failure, there is an energetic mismatch between metabolic demand and supply. Numerous measures of mitochondrial function have been made in failing myocardium of animal models and humans, with reports of decreased activity Krebs cycle enzymes and respiratory complexes, decreased levels of free CoQ, reduced expression of F(0)F(1)-ATPase, reduction in mitochondrial supercomplex assembly, increased ROS production, among others extensively reviewed elsewhere [4]. Controversy in the field still exists regarding whether or not the energetic deficiency in HF is due to insufficient ATP production by the mitochondria or defective/deficient creatine kinase activity; a cause/effect conundrum which continues to elude and is further obscured by the metabolic plasticity of the heart [55, 56]. Downregulation of genes that encode for fatty acid oxidation enzymes has been previously reported in the failing heart [57] driving a metabolic switch towards glycolysis, although this is more evident in late stages of HF [58]. In contrast, the loss of functional cardiomyocytes with acute I/R alters the load distribution in the heart, which may partially explain the lack of differences in fatty acid-supported respiration within our model. However, JO_2 was indeed lower in the presence of both fatty acid and carbohydrate substrates, being reversed by EA1 administration. It is noteworthy to mention that when the ability of the mitochondria to

generate membrane potential and produce ATP were tested in the isolated organelle, no differences were observed between *sham* and I/R (Figure 6), contradicting previous reports of decreased ATP synthetic efficiency [59]. Furthermore, although mitochondrial ROS production is known to play a role in I/R injury [4], there were no changes in H_2O_2 production in PmFBs with I/R +/- EA1. Although the former reflects only H_2O_2 emission potential, and not precisely H_2O_2 emission during the I/R insult, it is likely that EA1-mediated actions on mitochondrial function are independent of ROS emission potential. Indeed, thermodynamic assessment of the force-flow relation revealed a decrease in OXPHOS conductance with I/R that was fully reversed by EA1 administration. To our knowledge, this is the first time these types of measurements have been made in a model of cardiac I/R injury. It is worth to keep in mind however, that the present observations took place during the early stages of repair (at 24 hrs), and thus may not be necessarily transferable to later stages of I/R recovery.

In the heart, the mitochondrial network is extensively connected physically and electrically, allowing for distribution of nutrients and membrane potential, as well as enabling rapid signaling from damaged areas of the network [60, 10]. HF has been associated with fragmentation of the mitochondrial network, presenting reduced organelle size and increased mitochondria number of compromised structural integrity [39]. Analysis of TEM images revealed a clear trend in interfibrillar mitochondrial disorganization within the sarcomeres with I/R, that was prevented with EA1 administration (Figure 3). The primary impact on interfibrillar mitochondria *versus* the subsarcolemmal population was evident from the finding that the changes reported in respiration in PmFBs disappeared in the isolated organelle (Figure 6). The higher expression levels of ChChd3 with EA1 treatment also suggests better mitochondrial cristae integrity and mitochondrial function. In addition, the marked increase in certain fission markers (Drp1 and Fis1) further points to a more favorable balance towards fission, which could potentially be related to enhanced mitophagy [61] and therefore prevention of apoptotic signals. Although we did not evaluate activation of mitophagy pathways, this may partly explain the previously reported EA1-induced attenuation of apoptosis and enhanced autophagy [13]. Additionally, we observed a reduction in the accumulation of lipid droplets in EA1-treated myocardium, suggestive of reduced lipotoxicity, however, the composition of these droplets and the associated metabolic machinery must be investigated further [62, 63]. Overall, EA1 appears to mediate effects in the interfibrillar mitochondrial network ultra-structure, helping maintain its spatial organization within the cardiomyocytes and thus preserving the electrical "power grid" [10, 64] to endure the ischemic insult.

The ability of a terminally differentiated cardiomyocyte to withstand an ischemic insult is tightly linked to its bioenergetics and cellular ultrastructure [65, 15]. Mitochondrial function relies heavily on the cytoskeleton for structural support, localization and motility [66]. In fact, severe changes in cytoskeleton morphology and myocardial ultrastructure are known to correlate with reduced myocardial function and chronic heart failure (HF) [41]. EphrinA1-EphR signaling normally regulates several aspects of cell differentiation, proliferation, and migration [54, 67]. Interestingly, Ephrin-EphR signaling is known to affect cytoskeleton dynamics, enabling cell migration and adhesion, with emerging evidence pointing to a direct role in the regulation of actin-myosin interactions [68, 69]. Accompanied by remarkable preservation of OXPHOS kinetics, it was evident from TEM imaging that EA1 exerted a direct impact on cardiomyocyte ultra-structure, affecting sarcomere and Z-disks alignment. Thus, it is possible that the protective effects of EA1 in mitochondrial bioenergetics could be mediated via the cytoskeleton.

The microtubules (MTs) are highly dynamic structures of the cytoskeleton that play a key role in cell division and structural support for the cytoplasm, as well as serve as railroads for cellular trafficking of proteins and organelles, including mitochondria [70]. Several aspects of mitochondrial shape [48], fission-fusion dynamics [71], as well as function [47] are tightly linked to MT dynamics. Given EA1 is a ligand for the tyrosine kinase receptors EPH, an extensive phosphorylation cascade likely triggers and modulates a complex cellular response upon I/R injury. Interestingly, the phosphorylation status of α-tubulin, the unit component of the microtubules, appeared to be affected by I/R +/- EA1, thereby suggestive of a highly potential direct target of EA1 action (Figure 8).

Phosphorylation of α-tubulin at specific tyrosine residues (i.e. Tyr 272) prevents its polymerization into MTs [49, 72]. A certain degree of MT dynamics may be important for cardiomyocyte survival under I/R stress, as transport of mitochondria to high-risk injured cardiomyocytes prevents apoptosis [73], and inhibition of MT dynamics hinders repair after acute I/R injury in kidney [74]. Considering the EphA-R(s) are receptor tyrosine kinases, by increasing phosphorylation of α-tubulin, we may speculate EA1 protects mitochondrial bioenergetics via preservation of MT dynamics and thereby mitochondrial organization and function. In addition, phosphorylation of different

552 components of the electron transport system (ETS) has been known to modulate efficiency of mitochondrial
553 function [75]. EA1/EphA-induced phosphorylation pathway likely targets components of the cytoskeleton as well as
554 the ETS to preserve mitochondrial bioenergetics. Further investigation of the EphrinA1-mediated actions on the
555 cytoskeleton and mitochondrial structure/function are warranted to fully elucidate the mechanistic pathways by
556 which EA1 limits tissue damage and preserves cardiac function during I/R.
557
558 **Conclusions**
559 The present findings suggest administration of EA1 at the time of I/R protects cardiac function during early stages of
560 repair, by preservation of the mitochondrial network structure and bioenergetics. Current efforts are directed to
561 elucidating the EA1/EphA signaling pathway(s) that link the timing of post-translational modifications of
562 cytoskeletal components with mitochondrial function and other cell survival processes as well as region-specific
563 changes in contractile function relative to the occlusion. This includes the identification of the specific EphA
564 receptor(s) involved, their signaling targets, and how they change as a function of reperfusion time. Once the
565 mechanistic pathway of action is fully elucidated, EA1 may emerge as a potential novel therapeutic for the treatment
566 of acute I/R injury to prevent heart failure.
567
568
569 **Acknowledgements**
570 We would like to acknowledge the departments of Physiology, Anatomy and Cell Biology, Kinesiology, the East
571 Carolina Diabetes and Obesity Institute, and Comparative Medicine for their support and technical assistance. This
572 work was supported by US Public Health Services grants 1RH15HL124483-01A1 (J.A.I.V.), R01 DK096907 and
573 DK110656 (P.D.N.), and R01 AR070200 (J.J.B.).
574
575

References

1. Benjamin EJ, Virani SS, Callaway CW, Chang AR, Cheng S, Chiuve SE et al. Heart Disease and Stroke Statistics-2018 Update: A Report From the American Heart Association. Circulation. 2018. doi:10.1161/CIR.0000000000000558.
2. Yellon DM, Hausenloy DJ. Myocardial reperfusion injury. N Engl J Med. 2007;357(11):1121-35. doi:10.1056/NEJMra071667.
3. Lassen JF, Botker HE, Terkelsen CJ. Timely and optimal treatment of patients with STEMI. Nat Rev Cardiol. 2013;10(1):41-8. doi:10.1038/nrcardio.2012.156.
4. Brown DA, Perry JB, Allen ME, Sabbah HN, Stauffer BL, Shaikh SR et al. Expert consensus document: Mitochondrial function as a therapeutic target in heart failure. Nat Rev Cardiol. 2017;14(4):238-50. doi:10.1038/nrcardio.2016.203.
5. Murphy E, Ardehali H, Balaban RS, DiLisa F, Dorn GW, 2nd, Kitsis RN et al. Mitochondrial Function, Biology, and Role in Disease: A Scientific Statement From the American Heart Association. Circ Res. 2016;118(12):1960-91. doi:10.1161/RES.0000000000000104.
6. Heusch G. Molecular basis of cardioprotection: signal transduction in ischemic pre-, post-, and remote conditioning. Circ Res. 2015;116(4):674-99. doi:10.1161/CIRCRESAHA.116.305348.
7. Lesnefsky EJ, Chen Q, Tandler B, Hoppel CL. Mitochondrial Dysfunction and Myocardial Ischemia-Reperfusion: Implications for Novel Therapies. Annu Rev Pharmacol Toxicol. 2017;57:535-65. doi:10.1146/annurev-pharmtox-010715-103335.
8. Consolini AE, Ragone MI, Bonazzola P, Colareda GA. Mitochondrial Bioenergetics During Ischemia and Reperfusion. Adv Exp Med Biol. 2017;982:141-67. doi:10.1007/978-3-319-55330-6_8.
9. Lopaschuk GD. Metabolic Modulators in Heart Disease: Past, Present, and Future. Can J Cardiol. 2017;33(7):838-49. doi:10.1016/j.cjca.2016.12.013.
10. Glancy B, Hartnell LM, Combs CA, Fenmou A, Sun J, Murphy E et al. Power Grid Protection of the Muscle Mitochondrial Reticulum. Cell Rep. 2017;19(3):487-96. doi:10.1016/j.celrep.2017.03.063.
11. Walters AM, Porter GA, Jr., Brookes PS. Mitochondria as a drug target in ischemic heart disease and cardiomyopathy. Circ Res. 2012;111(9):1222-36. doi:10.1161/CIRCRESAHA.112.265660.
12. Dries JL, Kent SD, Virag JA. Intramyocardial administration of chimeric ephrinA1-Fc promotes tissue salvage following myocardial infarction in mice. The Journal of physiology. 2011;589(Pt 7):1725-40. doi:10.1113/jphysiol.2010.202366.
13. DuSablon A, Parks J, Whitehurst K, Estes H, Chase R, Vlahos E et al. EphrinA1-Fc attenuates myocardial ischemia/reperfusion injury in mice. PloS one. 2017;12(12):e0189307. doi:10.1371/journal.pone.0189307.
14. Horton JL, Virag J. Use of Multifactorial Treatments to Address the Challenge of Translating Experimental Myocardial Infarct Reduction Strategies. Int J Mol Sci. 2019;20(6). doi:10.3390/ijms20061449.
15. Saks V, Guzun R, Timohhina N, Tepp K, Varikmaa M, Monge C et al. Structure-function relationships in feedback regulation of energy fluxes in vivo in health and disease: mitochondrial interactosome. Biochim Biophys Acta. 2010;1797(6-7):678-97. doi:10.1016/j.bbabio.2010.01.011.
16. Virag JA, Lust RM. Coronary artery ligation and intramyocardial injection in a murine model of infarction. Journal of visualized experiments : JoVE. 2011(52). doi:10.3791/2581.
17. Bhan A, Sirker A, Zhang J, Protti A, Catibog N, Driver W et al. High-frequency speckle tracking echocardiography in the assessment of left ventricular function and remodeling after murine myocardial infarction. American journal of physiology Heart and circulatory physiology. 2014;306(9):H1371-83. doi:10.1152/ajpheart.00553.2013.

18. Lindsey ML, Kassiri Z, Virag JAI, de Castro Bras LE, Scherrer-Crosbie M. Guidelines for measuring cardiac physiology in mice. American journal of physiology Heart and circulatory physiology. 2018;314(4):H733-H52. doi:10.1152/ajpheart.00339.2017.
19. Busada JT, Kaye EP, Renegar RH, Geyer CB. Retinoic acid induces multiple hallmarks of the prospermatogonia-to-spermatogonia transition in the neonatal mouse. Biol Reprod. 2014;90(3):64. doi:10.1095/biolreprod.113.114645.
20. Kalkhoran SB, Munro P, Qiao F, Ong SB, Hall AR, Cabrera-Fuentes H et al. Unique morphological characteristics of mitochondrial subtypes in the heart: the effect of ischemia and ischemic preconditioning. Discoveries (Craiova). 2017;5(1). doi:10.15190/d.2017.1.
21. Picard M, Azuelos I, Jung B, Giordano C, Matecki S, Hussain S et al. Mechanical ventilation triggers abnormal mitochondrial dynamics and morphology in the diaphragm. J Appl Physiol (1985). 2015;118(9):1161-71. doi:10.1152/japplphysiol.00873.2014.
22. Torres MJ, Kew KA, Ryan TE, Pennington ER, Lin CT, Buddo KA et al. 17beta-Estradiol Directly Lowers Mitochondrial Membrane Microviscosity and Improves Bioenergetic Function in Skeletal Muscle. Cell Metab. 2017. doi:10.1016/j.cmet.2017.10.003.
23. Glancy B, Willis WT, Chess DJ, Balaban RS. Effect of calcium on the oxidative phosphorylation cascade in skeletal muscle mitochondria. Biochemistry (Mosc). 2013;52(16):2793-809. doi:10.1021/bi3015983.
24. Fisher-Wellman KH, Davidson MT, Narowski TM, Lin CT, Koves TR, Muoio DM. Mitochondrial Diagnostics: A Multiplexed Assay Platform for Comprehensive Assessment of Mitochondrial Energy Fluxes. Cell Rep. 2018;24(13):3593-606 e10. doi:10.1016/j.celrep.2018.08.091.
25. Frezza C, Cipolat S, Scorrano L. Organelle isolation: functional mitochondria from mouse liver, muscle and cultured fibroblasts. Nat Protoc. 2007;2(2):287-95. doi:10.1038/nprot.2006.478.
26. Lark DS, Torres MJ, Lin CT, Ryan TE, Anderson EJ, Neufer PD. Direct real-time quantification of mitochondrial oxidative phosphorylation efficiency in permeabilized skeletal muscle myofibers. Am J Physiol Cell Physiol. 2016;311(2):C239-45. doi:10.1152/ajpcell.00124.2016.
27. Fisher-Wellman KH, Lin CT, Ryan TE, Reese LR, Gilliam LA, Cathey BL et al. Pyruvate dehydrogenase complex and nicotinamide nucleotide transhydrogenase constitute an energy-consuming redox circuit. Biochem J. 2015;467(2):271-80. doi:10.1042/BJ20141447.
28. Brault JJ, Pizzimenti NM, Dentel JN, Wiseman RW. Selective inhibition of ATPase activity during contraction alters the activation of p38 MAP kinase isoforms in skeletal muscle. J Cell Biochem. 2013;114(6):1445-55. doi:10.1002/jcb.24486.
29. O'Neal WT, Griffin WF, Dries-Devlin JL, Kent SD, Chen J, Willis MS et al. Ephrin-Eph signaling as a potential therapeutic target for the treatment of myocardial infarction. Med Hypotheses. 2013;80(6):738-44. doi:10.1016/j.mehy.2013.02.024.
30. Gianni D, Chan J, Gwathmey JK, del Monte F, Hajjar RJ. SERCA2a in heart failure: role and therapeutic prospects. J Bioenerg Biomembr. 2005;37(6):375-80. doi:10.1007/s10863-005-9474-z.
31. Park WJ, Oh JG. SERCA2a: a prime target for modulation of cardiac contractility during heart failure. BMB Rep. 2013;46(5):237-43.
32. Samuel TJ, Rosenberry RP, Lee S, Pan Z. Correcting Calcium Dysregulation in Chronic Heart Failure Using SERCA2a Gene Therapy. Int J Mol Sci. 2018;19(4). doi:10.3390/ijms19041086.
33. Talukder MA, Kalyanasundaram A, Zuo L, Velayutham M, Nishijima Y, Periasamy M et al. Is reduced SERCA2a expression detrimental or beneficial to postischemic cardiac function and injury? Evidence from heterozygous SERCA2a knockout mice. American journal of physiology Heart and circulatory physiology. 2008;294(3):H1426-34. doi:10.1152/ajpheart.01016.2007.
34. Talukder MA, Yang F, Nishijima Y, Chen CA, Kalyanasundaram A, Periasamy M et al. Reduced SERCA2a converts sub-lethal myocardial injury to infarction and affects postischemic functional recovery. J Mol Cell Cardiol. 2009;46(2):285-7. doi:10.1016/j.yjmcc.2008.10.026.

669 35. Darshi M, Mendiola VL, Mackey MR, Murphy AN, Koller A, Perkins GA et al. ChChd3, an inner
670 mitochondrial membrane protein, is essential for maintaining crista integrity and mitochondrial
671 function. J Biol Chem. 2011;286(4):2918-32. doi:10.1074/jbc.M110.171975.
672 36. Lee AS. The ER chaperone and signaling regulator GRP78/BiP as a monitor of endoplasmic reticulum
673 stress. Methods. 2005;35(4):373-81. doi:10.1016/j.ymeth.2004.10.010.
674 37. Biala AK, Kirshenbaum LA. The interplay between cell death signaling pathways in the heart. Trends
675 Cardiovasc Med. 2014;24(8):325-31. doi:10.1016/j.tcm.2014.08.002.
676 38. Maejima Y, Isobe M, Sadoshima J. Regulation of autophagy by Beclin 1 in the heart. J Mol Cell
677 Cardiol. 2016;95:19-25. doi:10.1016/j.yjmcc.2015.10.032.
678 39. Ide T, Tsutsui H, Hayashidani S, Kang D, Suematsu N, Nakamura K et al. Mitochondrial DNA damage
679 and dysfunction associated with oxidative stress in failing hearts after myocardial infarction. Circ Res.
680 2001;88(5):529-35.
681 40. Sabbah HN, Sharov V, Riddle JM, Kono T, Lesch M, Goldstein S. Mitochondrial abnormalities in
682 myocardium of dogs with chronic heart failure. J Mol Cell Cardiol. 1992;24(11):1333-47.
683 41. Schaper J, Froede R, Hein S, Buck A, Hashizume H, Speiser B et al. Impairment of the myocardial
684 ultrastructure and changes of the cytoskeleton in dilated cardiomyopathy. Circulation. 1991;83(2):504-
685 14.
686 42. Knowlton AA, Liu TT. Mitochondrial Dynamics and Heart Failure. Compr Physiol. 2015;6(1):507-26.
687 doi:10.1002/cphy.c150022.
688 43. Chen L, Gong Q, Stice JP, Knowlton AA. Mitochondrial OPA1, apoptosis, and heart failure. Cardiovasc
689 Res. 2009;84(1):91-9. doi:10.1093/cvr/cvp181.
690 44. Larsen S, Nielsen J, Hansen CN, Nielsen LB, Wibrand F, Stride N et al. Biomarkers of mitochondrial
691 content in skeletal muscle of healthy young human subjects. J Physiol. 2012;590(Pt 14):3349-60.
692 45. Lefort N, Glancy B, Bowen B, Willis WT, Bailowitz Z, De Filippis EA et al. Increased reactive oxygen
693 species production and lower abundance of complex I subunits and carnitine palmitoyltransferase 1B
694 protein despite normal mitochondrial respiration in insulin-resistant human skeletal muscle. Diabetes.
695 2010;59(10):2444-52. doi:10.2337/db10-0174.
696 46. Atkinson DE, Walton GM. Adenosine triphosphate conservation in metabolic regulation. Rat liver
697 citrate cleavage enzyme. J Biol Chem. 1967;242(13):3239-41.
698 47. Anesti V, Scorrano L. The relationship between mitochondrial shape and function and the
699 cytoskeleton. Biochim Biophys Acta. 2006;1757(5-6):692-9. doi:10.1016/j.bbabio.2006.04.013.
700 48. Sukhorukov VM, Meyer-Hermann M. Structural Heterogeneity of Mitochondria Induced by the
701 Microtubule Cytoskeleton. Sci Rep. 2015;5:13924. doi:10.1038/srep13924.
702 49. Wandosell F, Serrano L, Avila J. Phosphorylation of alpha-tubulin carboxyl-terminal tyrosine prevents
703 its incorporation into microtubules. J Biol Chem. 1987;262(17):8268-73.
704 50. Hollander JM, Thapa D, Shepherd DL. Physiological and structural differences in spatially distinct
705 subpopulations of cardiac mitochondria: influence of cardiac pathologies. Am J Physiol Heart Circ
706 Physiol. 2014;307(1):H1-14. doi:10.1152/ajpheart.00747.2013.
707 51. Boengler K, Stahlhofen S, van de Sand A, Gres P, Ruiz-Meana M, Garcia-Dorado D et al. Presence of
708 connexin 43 in subsarcolemmal, but not in interfibrillar cardiomyocyte mitochondria. Basic Res Cardiol.
709 2009;104(2):141-7. doi:10.1007/s00395-009-0007-5.
710 52. Hatano A, Okada J, Washio T, Hisada T, Sugiura S. Distinct functional roles of cardiac mitochondrial
711 subpopulations revealed by a 3D simulation model. Biophys J. 2015;108(11):2732-9.
712 doi:10.1016/j.bpj.2015.04.031.
713 53. Schwarzer M, Schrepper A, Amorim PA, Osterholt M, Doenst T. Pressure overload differentially
714 affects respiratory capacity in interfibrillar and subsarcolemmal mitochondria. Am J Physiol Heart Circ
715 Physiol. 2013;304(4):H529-37. doi:10.1152/ajpheart.00699.2012.

54. Boyd AW, Bartlett PF, Lackmann M. Therapeutic targeting of EPH receptors and their ligands. Nat Rev Drug Discov. 2014;13(1):39-62. doi:10.1038/nrd4175.
55. Tian R, Nascimben L, Kaddurah-Daouk R, Ingwall JS. Depletion of energy reserve via the creatine kinase reaction during the evolution of heart failure in cardiomyopathic hamsters. J Mol Cell Cardiol. 1996;28(4):755-65. doi:10.1006/jmcc.1996.0070.
56. Weiss RG, Gerstenblith G, Bottomley PA. ATP flux through creatine kinase in the normal, stressed, and failing human heart. Proc Natl Acad Sci U S A. 2005;102(3):808-13. doi:10.1073/pnas.0408962102.
57. Sack MN, Rader TA, Park S, Bastin J, McCune SA, Kelly DP. Fatty acid oxidation enzyme gene expression is downregulated in the failing heart. Circulation. 1996;94(11):2837-42.
58. Stanley WC, Recchia FA, Lopaschuk GD. Myocardial substrate metabolism in the normal and failing heart. Physiol Rev. 2005;85(3):1093-129. doi:10.1152/physrev.00006.2004.
59. Murray AJ, Cole MA, Lygate CA, Carr CA, Stuckey DJ, Little SE et al. Increased mitochondrial uncoupling proteins, respiratory uncoupling and decreased efficiency in the chronically infarcted rat heart. J Mol Cell Cardiol. 2008;44(4):694-700. doi:10.1016/j.yjmcc.2008.01.008.
60. Bakeeva LE, Chentsov Yu S, Skulachev VP. Intermitochondrial contacts in myocardiocytes. J Mol Cell Cardiol. 1983;15(7):413-20.
61. Frank M, Duvezin-Caubet S, Koob S, Occhipinti A, Jagasia R, Petcherski A et al. Mitophagy is triggered by mild oxidative stress in a mitochondrial fission dependent manner. Biochim Biophys Acta. 2012;1823(12):2297-310. doi:10.1016/j.bbamcr.2012.08.007.
62. Goldberg IJ, Reue K, Abumrad NA, Bickel PE, Cohen S, Fisher EA et al. Deciphering the Role of Lipid Droplets in Cardiovascular Disease: A Report From the 2017 National Heart, Lung, and Blood Institute Workshop. Circulation. 2018;138(3):305-15. doi:10.1161/CIRCULATIONAHA.118.033704.
63. D'Souza K, Nzirorera C, Kienesberger PC. Lipid metabolism and signaling in cardiac lipotoxicity. Biochim Biophys Acta. 2016;1861(10):1513-24. doi:10.1016/j.bbalip.2016.02.016.
64. Kurz FT, Derungs T, Aon MA, O'Rourke B, Armoundas AA. Mitochondrial networks in cardiac myocytes reveal dynamic coupling behavior. Biophys J. 2015;108(8):1922-33. doi:10.1016/j.bpj.2015.01.040.
65. Tuomainen T, Tavi P. The role of cardiac energy metabolism in cardiac hypertrophy and failure. Exp Cell Res. 2017;360(1):12-8. doi:10.1016/j.yexcr.2017.03.052.
66. Boldogh IR, Pon LA. Mitochondria on the move. Trends Cell Biol. 2007;17(10):502-10. doi:10.1016/j.tcb.2007.07.008.
67. Barquilla A, Pasquale EB. Eph receptors and ephrins: therapeutic opportunities. Annu Rev Pharmacol Toxicol. 2015;55:465-87. doi:10.1146/annurev-pharmtox-011112-140226.
68. Daoud A, Gopal U, Kaur J, Isaacs JS. Molecular and functional crosstalk between extracellular Hsp90 and ephrin A1 signaling. Oncotarget. 2017;8(63):106807-19. doi:10.18632/oncotarget.22370.
69. Krupke OA, Burke RD. Eph-Ephrin signaling and focal adhesion kinase regulate actomyosin-dependent apical constriction of ciliary band cells. Development. 2014;141(5):1075-84. doi:10.1242/dev.100123.
70. Barlan K, Gelfand VI. Microtubule-Based Transport and the Distribution, Tethering, and Organization of Organelles. Cold Spring Harb Perspect Biol. 2017;9(5). doi:10.1101/cshperspect.a025817.
71. Woods LC, Berbusse GW, Naylor K. Microtubules Are Essential for Mitochondrial Dynamics-Fission, Fusion, and Motility-in Dictyostelium discoideum. Front Cell Dev Biol. 2016;4:19. doi:10.3389/fcell.2016.00019.
72. Yu Y, Gaillard S, Phillip JM, Huang TC, Pinto SM, Tessarollo NG et al. Inhibition of Spleen Tyrosine Kinase Potentiates Paclitaxel-Induced Cytotoxicity in Ovarian Cancer Cells by Stabilizing Microtubules. Cancer Cell. 2015;28(1):82-96. doi:10.1016/j.ccell.2015.05.009.

762 73. Shen J, Zhang JH, Xiao H, Wu JM, He KM, Lv ZZ et al. Mitochondria are transported along
763 microtubules in membrane nanotubes to rescue distressed cardiomyocytes from apoptosis. Cell death &
764 disease. 2018;9(2):81. doi:10.1038/s41419-017-0145-x.
765 74. Han SJ, Kim JH, Kim JI, Park KM. Inhibition of microtubule dynamics impedes repair of kidney
766 ischemia/reperfusion injury and increases fibrosis. Sci Rep. 2016;6:27775. doi:10.1038/srep27775.
767 75. Stram AR, Payne RM. Post-translational modifications in mitochondria: protein signaling in the
768 powerhouse. Cell Mol Life Sci. 2016;73(21):4063-73. doi:10.1007/s00018-016-2280-4.

769

770

771

772

773

774

775

776 **Figure Legends**

777

778 **Figure 1. Experimental Model.** Graphical representation of left anterior descending coronary artery (LAD) ligation
779 depicting EA1/IgG intracardiac injection at border zone diffusing toward apex and transmurally as well as the
780 allocation of heart sections to the respective experimental endpoints. Two slices in the transversal plane were
781 collected for 1. transmission electron microscopy (TEM) and preparation of permeabilized fibers and isolated
782 mitochondria, and 2. metabolite analysis using UPLC and enzyme activity analyses.

783

784 **Figure 2. Protein levels of EphrinA1 (A), SERCA2a (B), chchd3 (C) and GRP78 (D) by western blotting.**
785 Representative blots are shown in the bottom. Bars are means +/- SEM and normalized to GAPDH levels. * $p<0.05$,
786 ** $p<0.005$, and *** $p<0.0005$ vs *sham*, and # $p<0.05$, ### $p<0.0005$ vs I/R from one-way ANOVA analysis. n=4
787 mice/group.

788

789 **Figure 3. EA1 administration in I/R helps preserve cardiomyocyte and mitochondrial 2-D ultrastructure. (A-**
790 **C)** Representative transmission electron microscopy (TEM) images from a section of left ventricle border infarct in
791 *sham*, and I/R+/-EA1, at x12,000 **(A)**, x20,000 **(B)**, and x40,000 **(c)** magnitude. Images captured with an EMSIS
792 MegaView G3 charge-coupled device digital camera. Scale bars: 2 µm in (A), 1 µm in (B) and 0.5 µm in (D). **(D-I)**
793 Analysis of morphological parameters in mitochondria (expressed in appropriate dimensions or arbitrary units):
794 surface area **(D)**, external perimeter **(E)**, aspect ratio **(F)**, form factor **(G)**, circularity **(H)**, roundness **(I)**, computed
795 as described in methods. **(J)** Number of electron-dense inter-mitochondrial junctions, and **(K)** lipid droplets. Bars
796 are means +/- SEM from averages of up to 18 images/mouse, n=3 for sham, and n=4-5 for I/R +/- EA1. *$p<0.05$
797 from one-way ANOVA analysis.

798

799 **Figure 4. Evaluation of mitochondrial dynamics.** Western blot analysis of Beclin1 **(A)**, Drp1 **(B)**, Fis1 **(C),** Opa1
800 **(D)**, and Mfn1 **(E).** Representative blots are shown in the bottom. Bars are means +/- SEM and normalized to
801 GAPDH levels. * $p<0.05$ vs sham, and # $p<0.05$ vs I/R from one-way ANOVA analysis. n=4 mice/group.

Figure 5. EA1 preserves mitochondrial bioenergetics in cardiac PmFBs. (A) Mitochondrial respiratory capacity measured in permeabilized fibers from left ventricle. Substrates added sequentially: 18 µM Palpmitoyl-carnitine (PC), 5 mM L-carnitine, 0.5 mM malate, 4 mM ADP, 10 mM pyruvate, 10 mM glutamate, 10 mM succinate. **(B)** Mitochondrial JH_2O_2 emitting potential measured after the addition of 10 mM succinate, and 1 µM BCNU + 1 µm auranufin (left panel), or 18 µM palmitoyl-carnitine, 5 mM L-carnitine and 1 µM BCNU + 1 µm auranufin (right panel). **(C)** Citrate synthase activity measured in homogenates of the PmFBs utilized in 3A and 3D. **(D)** Representative creatine kinase energetic clamp in PmFBs from LV after I/R +/- EA1. Steady-state JO_2 was measured and ΔG_{ATP} was calculated as described elsewhere, after each addition of PCr [23]. **(E)** Force-flow relationship where the slope represents conductance and the x-intercept the static head (ΔG_{ATP} at $JO_2 = 0$, represented at **(F)**). **(G)** ADP kinetics, showing data fitted to a Michaelis Menten function. **(H)** Eadie-Hofstee plot of the data presented in G, where $y = -(K_M ADP)x + Vmax$. Slopes (K_M) were not statistically different. Bars are means ± SEM. * $p<0.05$, ** $p<0.005$ vs. *sham* and # $p<0.05$ vs. I/R from one-way ANOVA analysis. N = 6-8 mice/group.

Figure 6. EA1-mediated protective effects in mitochondrial bioenergetics are not detected in the isolated organelle. (A) Enzymatic activities of key dehydrogenase enzymes in isolated mitochondria. Data are expressed as % of maximal rate value in each respective assay, n=3 mice/group**. (B and C)** Steady-state OXPHOS flux rates of O_2 consumption (B) and ATP production (C) were determined simultaneously in real-time using a glucose / hexokinase / glucose-phosphate dehydrogenase respiratory clamp after the sequential addition of 20 and 200 µM ADP. Respiration was supported by 0.5 mM malate, 5 mM pyruvate, 5 mM glutamate, 5 mM succinate. **(D)** Resulting ATP/O ratio calculated from steady-state $JATP/JO_2$. **(E)** Mitochondrial complex V enzymatic activity determined in isolated mitochondria. N=3 mice/group **(F)** Mitochondrial membrane potential determined using a TPP probe at different respiratory states via titration of malonate. **(G)** Mitochondrial respiratory capacity measured in isolated mitochondria from LV following the same protocol as in Figure 2A. Substrates added sequentially: 18 µM palmitoyl-carnitine (PC), 5 mM L-carnitine (carn), 0.5 mM malate (Mal), 4 mM ADP, 10 mM pyruvate (Pyr), 10 mM glutamate (glut), 10 mM succinate (succ). Values are means ± SEM, NS = no statistical differences found. N = 4 mice/group, with each data point representing a pooled sample from 2 mice.

Figure 7. Levels of metabolites determined by UPLC. Guanosine triphosphate GTP **(A)**, adenosine tri- **(B)**, di- **(C)** and mono-phosphate **(D)**, respective ATP/ADP **(E)** and ATP/AMP **(F)** ratios, adenine **(G)**, hypoxanthine **(H)**, IMP **(I)**, and total nucleotides **(J)**. Bars are means +/- SEM. No statistical differences were detected from a one-way ANOVA analysis. n = 9-15 mice/group.

Figure 8. EA1 administration in I/R preserves phosphorylation of α-Tubulin. Western blot analysis of α-Tubulin **(A)** and (Tyr272) phosphorylated-α-Tubulin **(B)** in LV homogenates. **(C)** Calculated p-α-Tubulin/ α-Tubulin ratio from a and b. Representative blots are shown on the right. Bars are means ± SEM, * $p<0.05$, ** $p<0.005$ vs. sham and ## $p<0.005$, ### $p<0.0005$ vs. I/R from one-way ANOVA analysis. N = 4 mice/group.

Elsevier
Radarweg 29
Amsterdam 1043 NX,
elsevier.com

Empowering Knowledge

Life Sciences

Conflict of Interest Policy

Article Title:

Intracardiac administration of ephrinA1-Fc preserves mitochondrial bioenergetics during acute ischemia/reperfusion injury

Author Names:

Maria J. Torres1, Kelsey L. McLaughlin1,2, Randall H. Renegar3, Smrithi Valsaraj2, K'Shylah S. Whitehurst2, Omar M. Sharaf2, Uma M. Sharma2, Julie L. Horton1,2, Brinda Sarathy2, Justin C. Parks2, Jeffrey J. Brault2,4, Kelsey H. Fisher-Wellman1,2, P. Darrell Neufer1,2, and Jitka A. I. Virag2†.

Declarations

Life Sciences require that the **corresponding author**, signs on behalf of all authors, a declaration of conflicting interests. If you have nothing to declare in any of these categories then this should be stated.

Conflict of Interest

A conflicting interest exists when professional judgment concerning a primary interest (such as patient's welfare or the validity of research) may be influenced by a secondary interest (such as financial gain or personal rivalry). It may arise for the authors when they have financial interest that may influence their interpretation of their results or those of others. Examples of potential conflicts of interest include employment, consultancies, stock ownership, honoraria, paid expert testimony, patent applications/registrations, and grants or other funding.

Please state any competing interests:

None

Funding Source

All sources of funding should also be acknowledged and you should declare any involvement of study sponsors in the study design; collection, analysis and interpretation of data; the writing of the manuscript; the decision to submit the manuscript for publication. If the study sponsors had no such involvement, this should be stated.

Please state any sources of funding for your research:

NIH

Elsevier

Radarweg 29

Amsterdam 1043 NX,

elsevier.com

Empowering Knowledge

Author Contribution to Study

All authors listed on your paper must have made significant contributions to the study. To ensure clarity, you are required to enter the specific details of each author's contribution, which must substantiate the inclusion of each person on the manuscript. Please detail this information below (submit additional sheets as necessary):

Author Name	Author Email	Specific Role in Study
Maria Torres and Jitka Virag	Maria J Torres <maria.torres.alcalde@duke.edu>; Renegar, Randall H <RENEGARRA@ecu.edu>; K'Shylah Whitehurst <whitehurstk14@students.ecu.edu>; Omar Sharaf omar.sharaf@gmail.com;	conception and design
Randy Renegar Smrithi Valsarj K'Shylah Whitehurst Omar Sharaf Just Parks	Justin Curtis Parks <justincurtisparks@gmail.com>; Jeffrey Brault <BRAULTJ@ECU.EDU>; Fisher-Wellman, Kelsey <FISHERWELLMANK17@ECU.EDU>; P. Darrell Neufer <NEUFERP@ecu.edu>; Julie Horton <juliehortonphd@gmail.com>; Kelsey McLaughlin <mclaughlink16@students.ecu.edu>; Brinda Sarathy <sarathyb16@students.ecu.edu>;	electron microscopy
Uma Sharma Jeffrey Brault Kelsey Fisher-Wellman Jitka Virag, Julie Horton, and Justin Parks Maria Torres and Kelsey McLaughlin	Uma Sharma <SHARMAU15@ECU.EDU>; Valsaraj, Smrithi <valsarajs13@students.ecu.edu>; Virag, Jitka <VIRAGJ@ecu.edu>	western blotting UPLC enzyme activities echocardiography mitochondrial function assays
Jitka Virag, Jeffrey Brault, and P. Darrell Neufer		funding acquisition
Smrithi Valsaraj, K'Shylah Whitehurst, Omar Sharaf, Brinda Sarath, and Justin Parks		logistics, validation, and visualization
Maria Torres Jeffrey Brault, Randy Renegar, Kelsey Fisher-Wellman, P. Darrell Neufer, and Jitka Virag		manuscript draft critical review
Jitka Virag		project administration

Signature

Jitka Virag

Digitally signed by Jitka Virag
DN: cn=Jitka Virag, o=East Carolina University, ou=Department of Physiology, Brody School of Medicine, email=viragj@ecu.edu, c=US
Date: 2019.09.12 17:18:02 -04'00'

Print name

Jitka Virag